



## ENHANCED SUPERCAPACITIVE PERFORMANCE OF NANOCRYSTALLINE $Mn_3O_4$ SYNTHESIZED BY HYDROTHERMAL METHOD

Dadamiah PMD Shaik<sup>a</sup>, P. Rosaiah<sup>b</sup> and O M Hussain\*

a. Department of Physics, Sree Vidyanikethan Engineering College, A. Rangampeta, Tirupathi, Andhra Pradesh, India

[rahilsp@gmail.com](mailto:rahilsp@gmail.com)


b,\*. Department of Physics, Thin film Laboratory, S V University, Tirupathi, Andhra Pradesh, India

[hussainsvu@gmail.com](mailto:hussainsvu@gmail.com)

### ABSTRACT

$Mn_3O_4$  nanoparticles have been successfully synthesized by a simple hydrothermal method at low temperatures. The processing conditions such as reaction temperature and time were optimized to synthesized phase pure nanocrystalline  $Mn_3O_4$  with good electrochemical properties. The particles synthesized at a reaction temperature of 150°C for 12 h exhibited different characteristic peaks along with (211) predominant orientation which corresponds to tetragonal structure of  $Mn_3O_4$  with space group  $I4_1/amd$  (141) and estimated crystallite size of 32 nm. The SEM analysis reveals that the octahedral shape of grains with an average grain size of 180 nm. The vibrational studies from Raman and FTIR measurements confirmed the microstructure and presence of Mn-O bonding. The conductivity of the product was increased with increasing temperature following the Arrhenius behavior with estimated activation energy of 0.37 eV. The supercapacitive performance of nanocrystalline  $Mn_3O_4$  octahedrons in 1M  $Na_2SO_4$  aqueous electrolyte exhibited a high specific capacitance of 348  $Fg^{-1}$  at current density of 0.5  $mAcm^{-2}$  and 70% capacitive retention even after 4000 cycles.

**Keywords:-**  $Mn_3O_4$  nanoparticles; hydrothermal method; activation energy; specific capacitance



## Council for Innovative Research

Peer Review Research Publishing System

**Journal:** Journal of Advances in Chemistry

Vol. 12, No. 1

[www.cirjac.com](http://www.cirjac.com)

[editorjaconline@gmail.com](mailto:editorjaconline@gmail.com), [editor@cirjac.com](mailto:editor@cirjac.com)



## 1. Introduction:

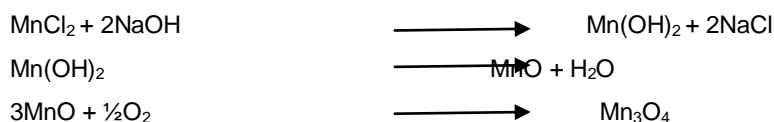
In recent days, the development of electrical energy storage devices is a very big challenge to meet the future energy requirements for microelectronic devices. Supercapacitors are the type of energy storage devices that have the advantages of high power density, friendly environment, high safety and convenient operation over a wide range of temperature. Supercapacitors are classified into two types based on charge storage mechanism as Electric Double Layer Capacitors (EDLC) and pseudo capacitors. The charge storage in EDLC is due to the accumulation of charges at electrode and electrolyte interface and in pseudo capacitors, it is due to the charge transfer from reversible Faradic reactions that takes place on the electrode surface. The performance of supercapacitors depends on the properties of electrode material used. Hence, many researchers were focused in development of new electrode materials for supercapacitors from the past few decades. In this perspective, activated carbon [1], Carbon Nano Tubes [2], conducting polymers [3, 4], and transition metal oxides [5] were used as electrode material for supercapacitor applications. Among these electrode materials, transition metal oxides play a very important role due to their high redox pseudo capacitance and chemical stability. Several transition metal oxides were used as the electrode materials for supercapacitors, such as RuO<sub>2</sub> [6], Co<sub>3</sub>O<sub>4</sub> [7], NiO [8], SnO<sub>2</sub> [9], CuO [10] and oxides of manganese [11-13]. Among these electrode materials, RuO<sub>2</sub> was the most widely studied material due to its high specific capacitance, high conductivity and excellent chemical stability. However, due to its high cost, less abundance and toxicity the usage of RuO<sub>2</sub> becomes difficult for practical applications. Manganese oxides with different crystalline structures become alternate electrode materials for supercapacitor applications due to their high theoretical specific capacitance, high power density, environmentally friendly nature, natural abundance, low cost and long term cyclic stability [14]. Manganese oxide crystallizes into MnO, Mn<sub>3</sub>O<sub>4</sub>, Mn<sub>2</sub>O<sub>3</sub> and MnO<sub>2</sub> due to the existence of three kinds of oxidation states of manganese (Mn<sup>2+</sup>, Mn<sup>3+</sup>, and Mn<sup>4+</sup>). Among these forms of manganese oxides, Mn<sub>3</sub>O<sub>4</sub> is one of the most stable and it has a variety of important applications in different areas including rechargeable lithium ion batteries, molecular adsorption, electrochemistry, magnetic and supercapacitors [15-18].

So far, Mn<sub>3</sub>O<sub>4</sub> nanoparticles were prepared and their supercapacitive behavior has been studied by many researches. For example, K Vijaya Shankar et al [19] prepared of Mn<sub>3</sub>O<sub>4</sub> nanoparticles using microwave assisted reflux synthesis method which exhibited specific capacitance of 74 Fg<sup>-1</sup> at a current density of 0.5 mAcm<sup>-2</sup> in 6M KOH. YANG Lu-Feng et al [20] reported a specific capacitance of 173 Fg<sup>-1</sup> at 0.2 Ag<sup>-1</sup> in 0.5M Na<sub>2</sub>SO<sub>4</sub> for Mn<sub>3</sub>O<sub>4</sub> Polyhedral nanocrystals prepared by solution based thermolysis process. H. Jiang et al [21] using hydrothermal synthesis prepared Mn<sub>3</sub>O<sub>4</sub> nano-octahedrons with specific capacitance of 322 Fg<sup>-1</sup> at a scan rate of 5 mVs<sup>-1</sup> in 1M Na<sub>2</sub>SO<sub>4</sub>. A high specific capacitance of 322 Fg<sup>-1</sup>, with 77% of capacitance retention after 1000 cycles was reported by B Gnana Sundara Raj et al [22] for Mn<sub>3</sub>O<sub>4</sub> nanospheres synthesized by chemical precipitation approach at a current density of 0.5 mAcm<sup>-2</sup> in 1M Na<sub>2</sub>SO<sub>4</sub>.

The supercapacitive performance of electrode materials mainly relies on size, shape, specific surface area, electrical conductivity, porous structure and crystalline nature which in turn depend on preparation methods. Among all chemical methods used for the preparation of Mn<sub>3</sub>O<sub>4</sub> nanoparticles, hydrothermal method is one of the best methods because it has a unique advantage of low temperature reaction and ability to create crystalline phases which are stable and particularly for the growth of good quality and control over their composition. Therefore, in the present investigation, hydrothermal method has been employed to synthesize Mn<sub>3</sub>O<sub>4</sub> crystalline particles with lower dimensions. It is noted that in hydrothermal method the particle size, shape and morphology of Mn<sub>3</sub>O<sub>4</sub> are influenced by reaction temperature and time. Hence, a detailed investigation has been carried out to understand the influence of reaction temperature and time on the growth of Mn<sub>3</sub>O<sub>4</sub>. It is demonstrated that the nanocrystalline Mn<sub>3</sub>O<sub>4</sub> electrode synthesized at 150°C for 12 h exhibited superior performance with high specific capacitance and excellent capacitive retention during cycling.

## 2. Experimental Procedure:

Manganese Chloride (MnCl<sub>2</sub>·4H<sub>2</sub>O) and Sodium Hydroxide (NaOH) were obtained from Merck co. and used without further purification. The solutions were prepared using double distilled (DD) water. In a typical preparation, 3.96g (1M) of MnCl<sub>2</sub>·4H<sub>2</sub>O was dissolved in 20 ml of DD water and 0.8g (1M) of NaOH was dissolved in 20 ml of DD water in separate beakers. The solution of manganese chloride was slowly added drop wise to the solution of sodium hydroxide under continuous stirring. The resultant solution was taken in a 50 ml Teflon lined stainless steel autoclave and kept at various temperatures (60°C – 180°C) and times (1 h - 24 h) in oven. The brown precipitates of Mn<sub>3</sub>O<sub>4</sub> were formed in the following steps



The autoclave was cooled to room temperature, brown precipitates were collected with centrifuge and cleaned with distilled water and ethanol for several times to remove the impurities followed by drying at 60°C for 24h.

Material Characterization:

The structural properties of as prepared nanocrystals were studied by Seifert X-ray diffractometer (Model 3003 TT ) using CuK<sub>α</sub> (λ=0.154nm) radiation source filtered by Ni thin film at a scan speed of 0.05° per second in the 2θ range 20°-80° and by Raman Spectroscopy using Horiba Jobin Yvon LabRAM HR800UV Raman Spectrometer with He-Ne laser 532 nm as an excitation wavelength. The morphology and chemical composition of the sample was analysed from carl



ZEISS (Model EVO MA15) in high vacuum and the chemical composition of the sample was analyzed by EDAX system (Oxford Instruments, UK)

Electrical studies:

The powder was pressed into 12 mm diameter pellet with 1 mm thickness and then annealed at 300°C for 4h. Silver paste is coated on both sides of the pellet for electrical measurements. The conductivity measurements were recorded on N4L PSM 1700, UK over the frequency range of 1 Hz to 1 MHz in the temperature range from room temperature to 373 K.

Electrochemical studies:

Firstly, working electrode was prepared from the mixture of Mn<sub>3</sub>O<sub>4</sub> powder (80%), carbon black (10%) and Poly Vinylidene Fluoride (10%) as binder. The above mixture was grinded for half an hour and then the homogenous slurry was made using N-methyl-2-pyrrolidone as a solvent. The slurry was subsequently brush-coated onto a chemically cleaned stainless steel plate. The electrode was dried at 100°C in air for 2h for the removal of the solvent.

A three electrode glass cell equipped with a Mn<sub>3</sub>O<sub>4</sub> working electrode, a platinum foil as counter and reference electrode and 1M Na<sub>2</sub>SO<sub>4</sub> as electrolyte used to study electrochemical behavior of Mn<sub>3</sub>O<sub>4</sub> nanoparticles. The electrochemical properties were examined on CHI608C electrochemical analyzer.

### 3. Result and Discussion:

#### 3.1. Microstructural Properties:

##### 3.1.1. XRD Analysis:

Fig.1a and 1b show the X-ray powder diffraction spectra of Mn<sub>3</sub>O<sub>4</sub> nanoparticles recorded in the diffraction angle 25°- 70° at different reaction temperatures(60°C -180°C) and times (1h-24h) respectively. The reaction was found to be incomplete below 150°C temperature. At temperature 150°C, the product exhibited predominant diffraction peak (211) along with characteristic (112), (200), (103), (004), (220), (204), (105), (312), (303), (321), (224), (440), (305), (413), (422), (404) peaks which corresponds to tetragonal structure of Mn<sub>3</sub>O<sub>4</sub> with I4<sub>1</sub>/amd(141) space group (JCPDS card No.89-4837). No other impurity peaks were detected in the spectra. By further increasing the reaction temperature, two impurities peaks at Bragg angle 29.15° and 37° were observed which belong to MnO<sub>2</sub> [23]. From Fig 1b it is observed that the peak intensities increased and the width of the peaks decreased as a function of reaction time. The coherent length (L<sub>c</sub>) which corresponds to the crystallite size of the sample was calculated from the predominant (211) diffraction peak for different reaction times using the following Debye-Scherrer's formula

Where, k is the Scherer's constant (0.94), λ is the wavelength of X ray radiation (1.5406Å), β is the full width at half maximum (FWHM) measured in radian and 'θ' is the corresponding Bragg angle. The calculated crystallite size was observed to be increased from 13 nm to 65 nm by increasing the reaction time from 1h to 24 h (Fig. 1c).

Vibrational studies:

The Raman spectroscopy is an effective characterization technique to investigate structure and chemical composition of the sample. The Raman spectra of the Mn<sub>3</sub>O<sub>4</sub> nanoparticles were recorded in the range 300-900 cm<sup>-1</sup> for different reaction times at 150°C as shown in Fig. 2. The common feature of these spectra is the presence of strong band around 650 cm<sup>-1</sup> and a group of bands between 200 cm<sup>-1</sup> - 500 cm<sup>-1</sup> with weaker intensity [24]. The main peak located at 654 cm<sup>-1</sup> corresponds to the Mn-O stretching vibrations (single degenerate A<sub>1g</sub> symmetry mode) of Mn<sup>2+</sup> in tetrahedral coordination. The two other peaks at 317 cm<sup>-1</sup> and 360 cm<sup>-1</sup> are assigned to the out of plane bending modes of Mn-O (E<sub>g</sub> symmetry mode) and asymmetric stretch of bridge oxygen species Mn-O-Mn respectively. One weak band at 462 cm<sup>-1</sup> is attributed to doubly degenerate T<sub>2g</sub> symmetry mode. All the peaks in the spectrum which are the representative for the tetragonal structure of Mn<sub>3</sub>O<sub>4</sub>. But, at lower reaction temperatures, the strong peak at 654 cm<sup>-1</sup> shifted and broadened. The red shift of the peak and peak broadening was mainly due to grain size effect [25, 26].

The vibrational studies of Mn<sub>3</sub>O<sub>4</sub> sample was also examined by FTIR within the wavenumber range of 2000-350 cm<sup>-1</sup> at a reaction temperature of 150°C for 12h in order to know the chemical bonds present in Mn<sub>3</sub>O<sub>4</sub> sample and is shown in Fig 3. The two broad peaks at 610 cm<sup>-1</sup> and 523 cm<sup>-1</sup> are associated with the Mn-O stretching mode of tetrahedral and octahedral site respectively. In addition, one broad absorption peak at 443 cm<sup>-1</sup> is attributed to vibration of manganese species in an octahedral site. The absorption peaks 1527 cm<sup>-1</sup> and 1038 cm<sup>-1</sup> may be attributed to O-H bending vibration combined with Mn atoms [27]. Thus, FTIR result shows the presence of Mn-O bonds confirming the formation of the Mn<sub>3</sub>O<sub>4</sub> product.

##### 3.1.2. SEM Analysis:

The effective surface area of the materials mainly depends on the size and shape of the nanoparticles which is very important for supercapacitor applications. The Mn<sub>3</sub>O<sub>4</sub> sample morphology was analyzed using SEM at reaction temperature of 150°C for three different reaction times as shown in Fig.4. At a reaction time of 1h, the sample consists of agglomerated nanograins with an average grain size of 100 nm. By increasing the reaction time from 1h to 12h, it is observed that the powder is composed of uniformly distributed octahedral shaped nanograins with an estimated average grain size of 180 nm (Fig4b). It can be clearly seen that the overlapped octahedral grains in inset of fig 4b. Further increasing the reaction time, the truncated octahedral shape of the particles was observed with increased size (Fig4d). The particle size obtained from SEM data is generally larger than the crystallite size obtained from XRD studies, so that



the primary particle size should not be confused with crystallite size. It may be noted that during the synthesis, the particles might have been assembled into primary particles with an average size of 180 nm [28].

The chemical composition of the sample has been carried out using EDAX measurement as shown in Fig.5. It exhibited corresponding binding energy peaks of Mn and O present in the sample and no other impurity peaks are detected in the spectrum which indicates the high chemical purity of the sample and the estimated compositions of Mn and O are 71.39% and 28.61% respectively.

### 3.1.3. Electrical Properties:

The impedance response of  $\text{Mn}_3\text{O}_4$  sample was studied from Cole-Cole plots at different temperatures as shown in Fig. 6. These plots allow the resistances related to grain interiors (bulk), grain boundaries and sample/electrode interfaces to be separated because each of them has different relaxation time, resulting in separate semicircles in the complex impedance plane. The relaxation frequency for the bulk is greater than the relaxation frequency for grain boundaries and the relaxation frequency resulting from the electrode process is much smaller than relaxation frequency of grain boundaries. As the temperature increases, all semicircles become smaller and shift towards higher-frequency region, indicating a reduction of grain ( $R_b$ ) and grain boundary resistance ( $R_{gb}$ ).

The temperature dependence of electrical conductivity in the range from room temperature to 373 K is as shown in Fig.7. It is clear that the conductivity increases with increasing temperature indicating semiconducting behavior of  $\text{Mn}_3\text{O}_4$  sample [29]. The electrical conductivity ( $\sigma$ ) of  $\text{Mn}_3\text{O}_4$  at 373 K was calculated using the formula  $\sigma = t/R_b A$ ,  $\text{Sm}^{-1}$  and is found to be  $1.86 \times 10^{-5} \text{Sm}^{-1}$ . Here,  $t$  is the thickness of the sample,  $R_b$  is the bulk resistance of the sample and  $A$  is the effective area. The conductivity data is fitted using the Arrhenius equation,  $\sigma = \sigma_0 \exp(-E_a/k_B T)$ , Here,  $\sigma_0$  is the pre exponential factor,  $E_a$  is activation energy in eV,  $k_B$  is Boltzmann constant and  $T$  is absolute temperature respectively. The activation energy was calculated from the above equation and is found to be 0.37 eV [30].

### 3.1.4. Electrochemical properties:

The electrochemical properties of  $\text{Mn}_3\text{O}_4$  nanoparticles were studied using Cyclic Voltammetry (CV), Chronopotentiometry (CP) and Electrochemical Impedance Spectroscopy (EIS) with three electrode glass cell equipped with a  $\text{Mn}_3\text{O}_4$  working electrode and platinum as counter and reference electrode in 1M  $\text{Na}_2\text{SO}_4$  aqueous electrolyte. Fig.8a shows the cyclic voltammograms of the  $\text{Mn}_3\text{O}_4$  nanoparticles at different scan rates from 1-50  $\text{mVs}^{-1}$  in the potential range -0.1V to +0.9V vs. Pt. It is observed that all the CV curves exhibited mirror image characteristics, which indicates that the Faraday redox reactions are electrochemically reversible representing an ideal electrochemical capacitor behavior. And also observed that the current under the curves is directly proportional to scan rate. The cycling performance is also important for electrochemical supercapacitor applications. The cyclic performance of  $\text{Mn}_3\text{O}_4$  electrode was studied from CV up to 1000 cycles at two different scan rates of 10  $\text{mVs}^{-1}$  and 20  $\text{mVs}^{-1}$  as is shown in Fig.8b. The CV curves are almost similar even after 1000 cycles indicates the  $\text{Mn}_3\text{O}_4$  electrode has high structural stability.

The galvanostatic charge–discharge cycling studies were carried out in 1M  $\text{Na}_2\text{SO}_4$  aqueous electrolyte in the potential range -0.1 V to +0.9 V vs. Pt to know more information about capacitive behavior of  $\text{Mn}_3\text{O}_4$  electrode. The  $\text{Mn}_3\text{O}_4$  nanoparticles show a sudden drop in potential at the starting of discharge [Fig. 9a] due to internal resistance. The linear variation of potential with time indicates the double-layer capacitance behavior, which is caused by the separation of charge at the electrode and electrolyte interface [31]. In addition, the internal resistance of  $\text{Mn}_3\text{O}_4$  electrode increases with increase in current density. The discharge specific capacitance of the sample was calculated from the following formula

$$C = \frac{I \Delta t}{\Delta V m}$$

Where  $C$  is specific capacitance in  $\text{Fg}^{-1}$ ,  $I$  is galvanostatic discharge current in A,  $\Delta t$  is the discharge time in s,  $\Delta V$  is the voltage range in V and  $m$  is the weight of the active material in the electrode in gram. The specific capacitance values are found to be 348  $\text{Fg}^{-1}$ , 330  $\text{Fg}^{-1}$ , 312  $\text{Fg}^{-1}$ , 298  $\text{Fg}^{-1}$  and 286  $\text{Fg}^{-1}$  at 0.5  $\text{mAcm}^{-2}$ , 1  $\text{mAcm}^{-2}$ , 2  $\text{mAcm}^{-2}$ , 3  $\text{mAcm}^{-2}$  and 5  $\text{mAcm}^{-2}$  respectively. The decrease of specific capacitance with increase in current density may be due to decrease in number of inner active sites of  $\text{Mn}_3\text{O}_4$  electrode contributed to the electrochemical reaction. The capacitive retention of  $\text{Mn}_3\text{O}_4$  electrode is about 82% with growth of current densities from 0.5  $\text{mAcm}^{-2}$  to 5  $\text{mAcm}^{-2}$ , indicating a good rate capability.

The cycling stability of  $\text{Mn}_3\text{O}_4$  nanoparticles was studied by galvanostatic charge–discharge cycling at a current density of 3  $\text{mAcm}^{-2}$  in 1M  $\text{Na}_2\text{SO}_4$  aqueous electrolyte within the potential range -0.1 V to +0.9 V vs. Pt as shown in Fig. 9b(first 10 cycles). The symmetry characteristic of the charge-discharge curves further support that the electrode has high electrochemical reversibility and excellent capacitive behavior. The specific capacitance decrease with cycle number as shown in Fig. 9c, and attains 70% capacitive retention after 4000 cycles. The decrease in capacitance is due to the loss of active sites in the electrode material during the early charging/discharging cycles in the electrolyte [12].

The Electrochemical Impedance Spectroscopy (EIS) analysis was carried out in 1M  $\text{Na}_2\text{SO}_4$  aqueous electrolyte at open circuit potential in the frequency range from 1Hz to 1MHz in order to study the capacitive behavior of the  $\text{Mn}_3\text{O}_4$  electrode material and also to confirm the CV result. The typical Nyquist plots of the  $\text{Mn}_3\text{O}_4$  nanoparticles before and after 4000 cycles are presented in Fig. 10. The intersection made on horizontal axis represents the solution resistance ( $R_s$ ) at high frequency region. It is observed that the solution resistance was increased from 1.14  $\Omega$  to 2.27  $\Omega$  after 4000 cycles. A semicircle in high to medium frequency region, which has been termed as a charge transfer resistance ( $R_{ct}$ ). The charge transfer resistance of the sample was increased from 30  $\Omega$  to 40  $\Omega$  after 4000 cycles. The increase in  $R_{ct}$  during cycling



suggests that the specific capacitance decrease with cycle number. The straight line behavior at low frequency region corresponds to Warburg impedance ( $R_w$ ) or diffusive resistance which indicates the characteristic behavior of supercapacitors.

#### 4. Conclusion:

$Mn_3O_4$  nanoparticles were successfully synthesized by a simple and low temperature hydrothermal technique at various reaction temperatures and time without the use of any surfactants for supercapacitor applications. The XRD spectra of  $Mn_3O_4$  nanoparticles synthesized at  $150^\circ C$  for 12 h, exhibited characteristic peaks along with (211) predominant orientation peak which corresponds to the tetragonal structure of  $Mn_3O_4$  with  $I4_1/amd$  (141) space group and the estimated crystallite size of 32 nm. The vibrational studies from Raman and FTIR confirmed the presence of Mn-O bonding. From SEM analysis the morphology of the sample was observed to be changes with reaction time and obtained octahedral shape of grains with an average grain size of 180 nm. The temperature dependent conductivity proves the semiconducting nature of  $Mn_3O_4$  nanoparticles and the estimated activation energy is 0.37 eV. The electrochemical behavior of  $Mn_3O_4$  nanoparticles were investigated using CV, Cronopotentiometry and EIS. The as prepared  $Mn_3O_4$  nanoparticles exhibited highest specific capacitance of  $348\text{ Fg}^{-1}$  at current density of  $0.5\text{ mAcm}^{-2}$  in  $1\text{M Na}_2\text{SO}_4$  aqueous electrolyte which may be due to high crystallinity, low particle size and octahedral shape. The superior performance of nanocrystalline  $Mn_3O_4$  electrode with 70% capacitive retention after 4000 cycles has a promising application in supercapacitors.

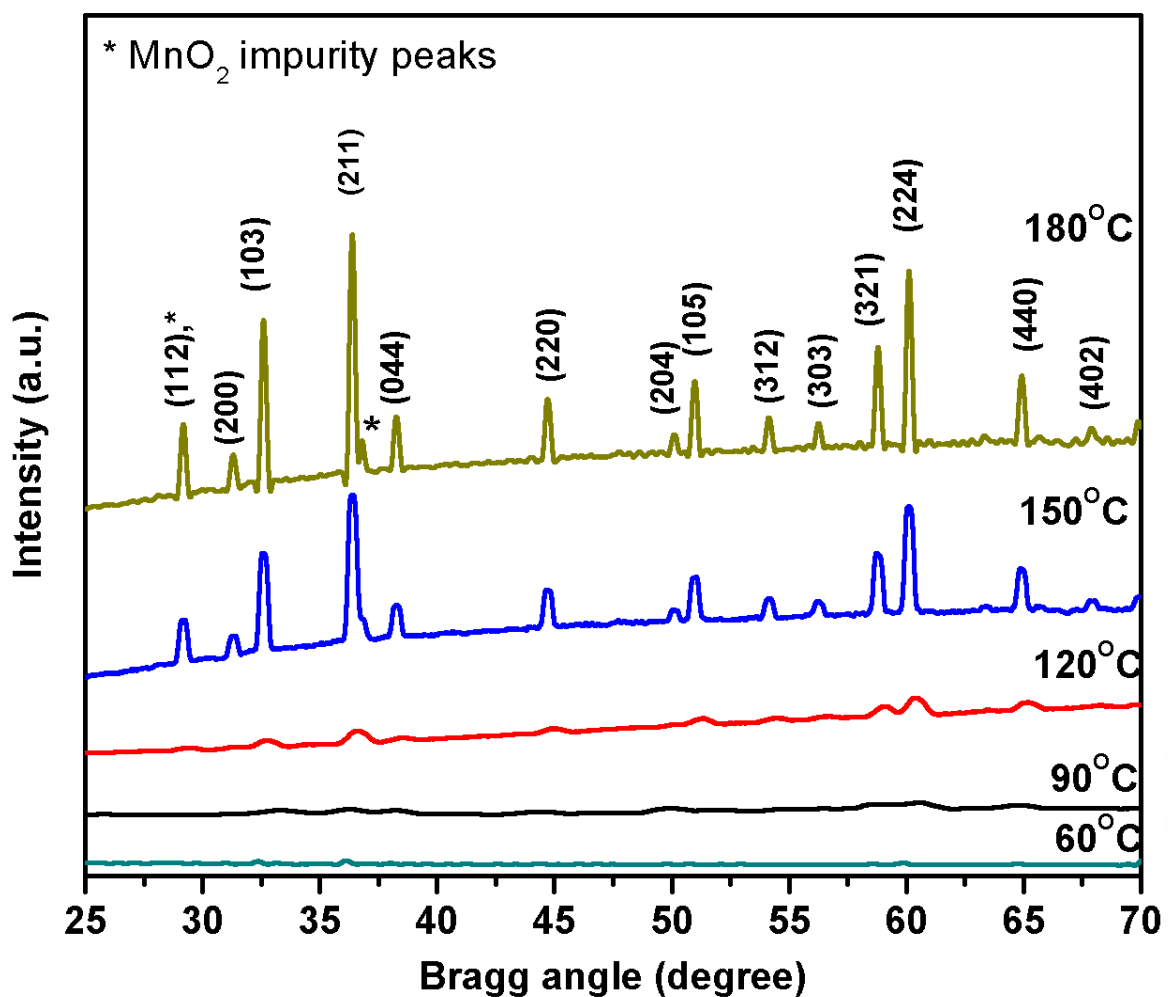


Fig.1a XRD spectrum of  $Mn_3O_4$  nanoparticles at different temperatures

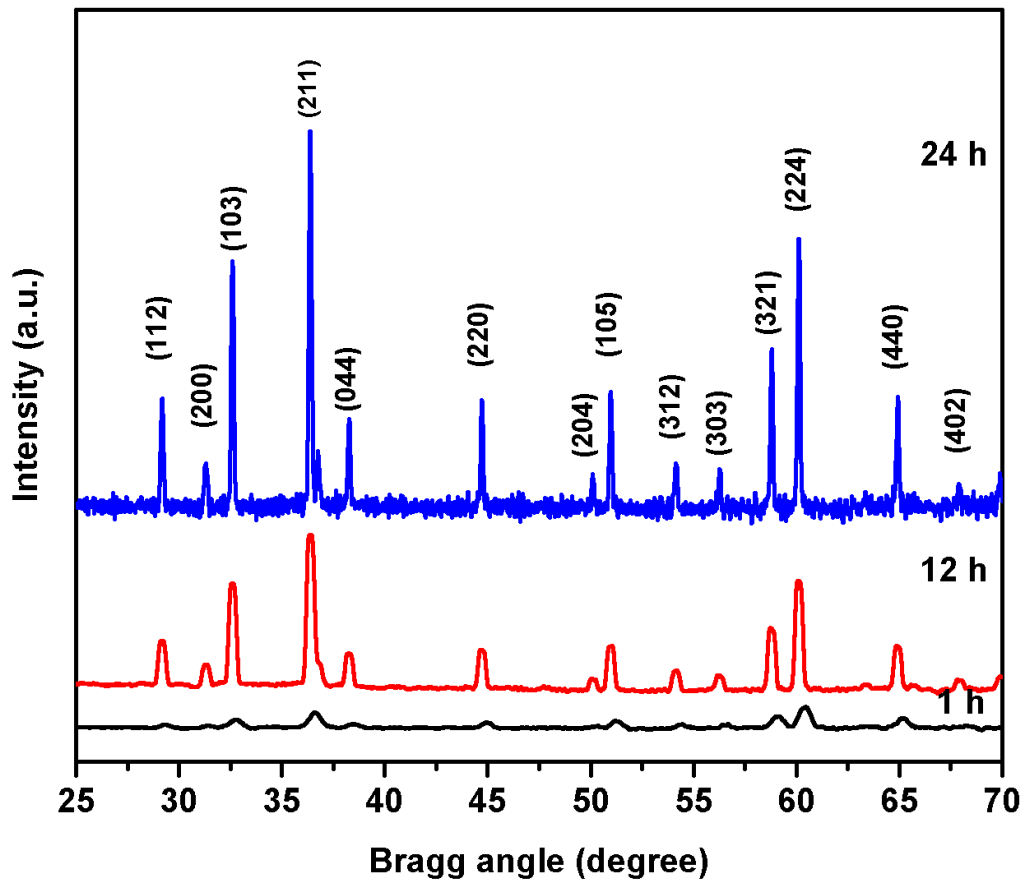


Fig 1b XRD at 150°C for different reaction times

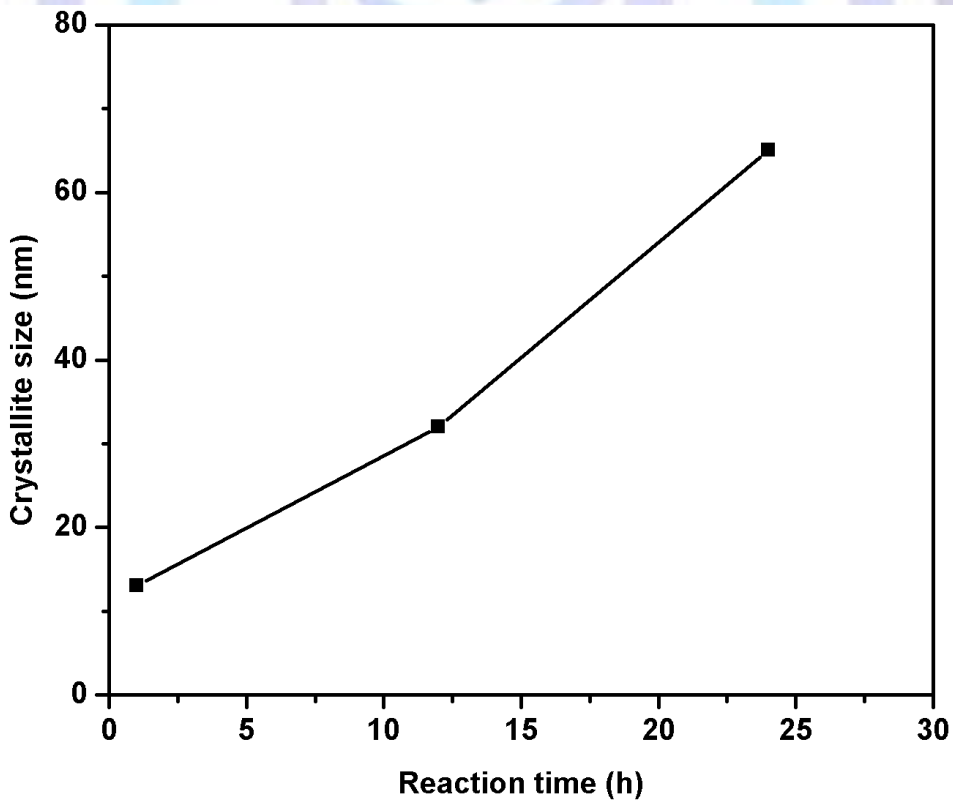


Fig 1c Crystallite size with reaction time at 150°C

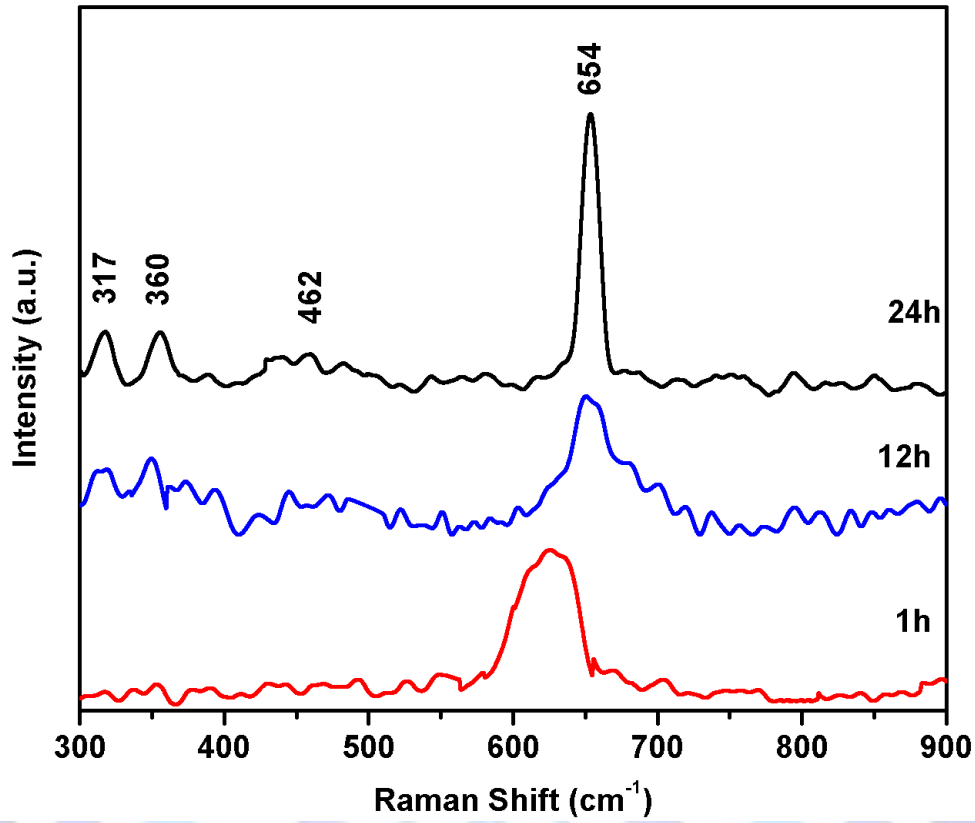


Fig.2 Raman spectra of Mn<sub>3</sub>O<sub>4</sub> nanoparticles

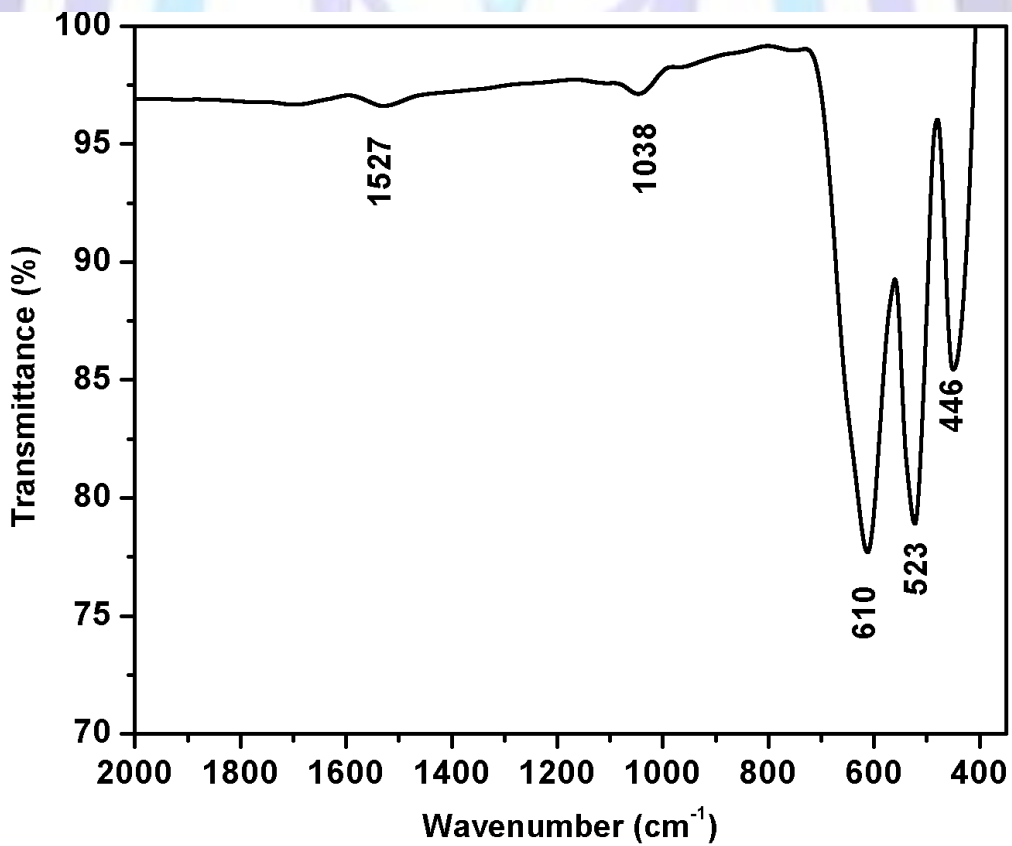


Fig.3 FT-IR spectra of Mn<sub>3</sub>O<sub>4</sub> nanoparticles

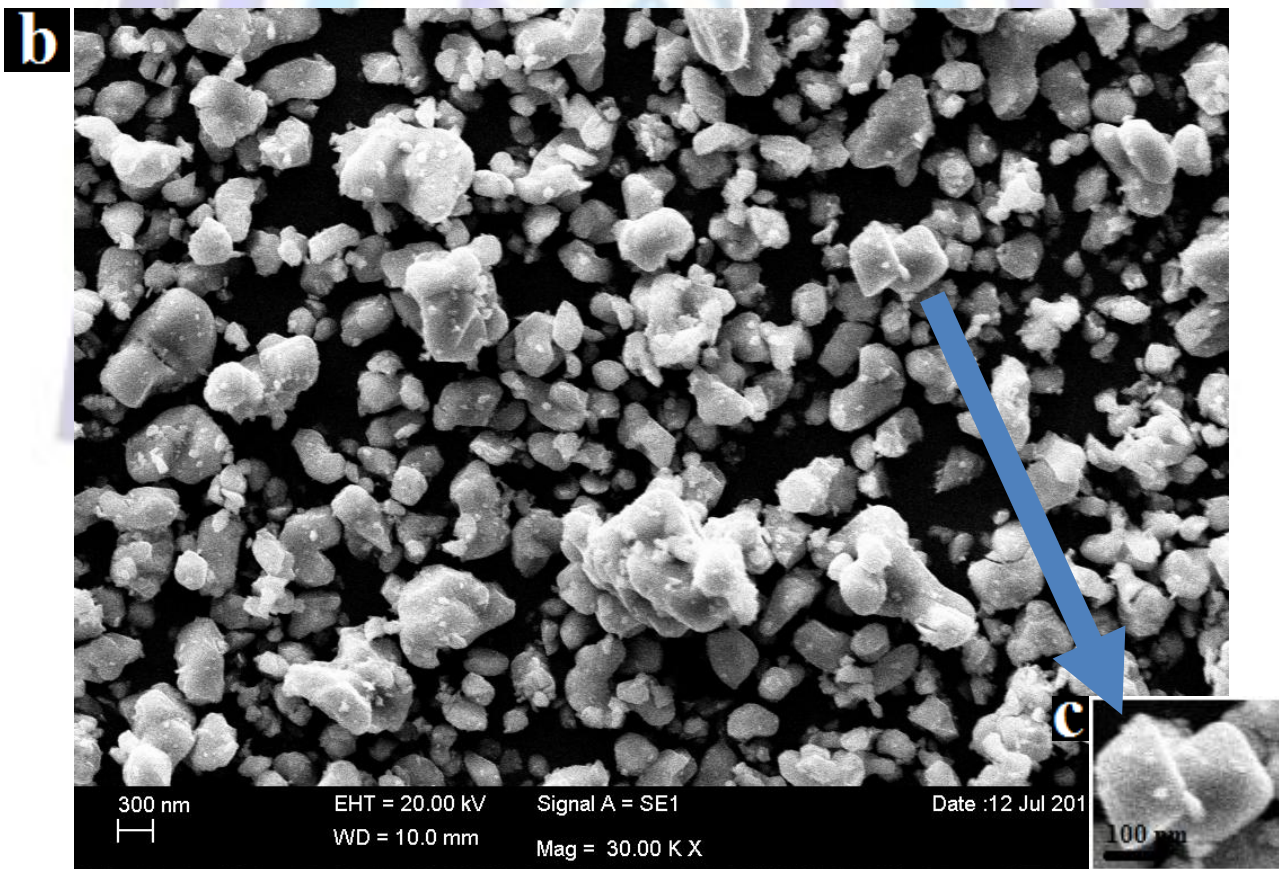
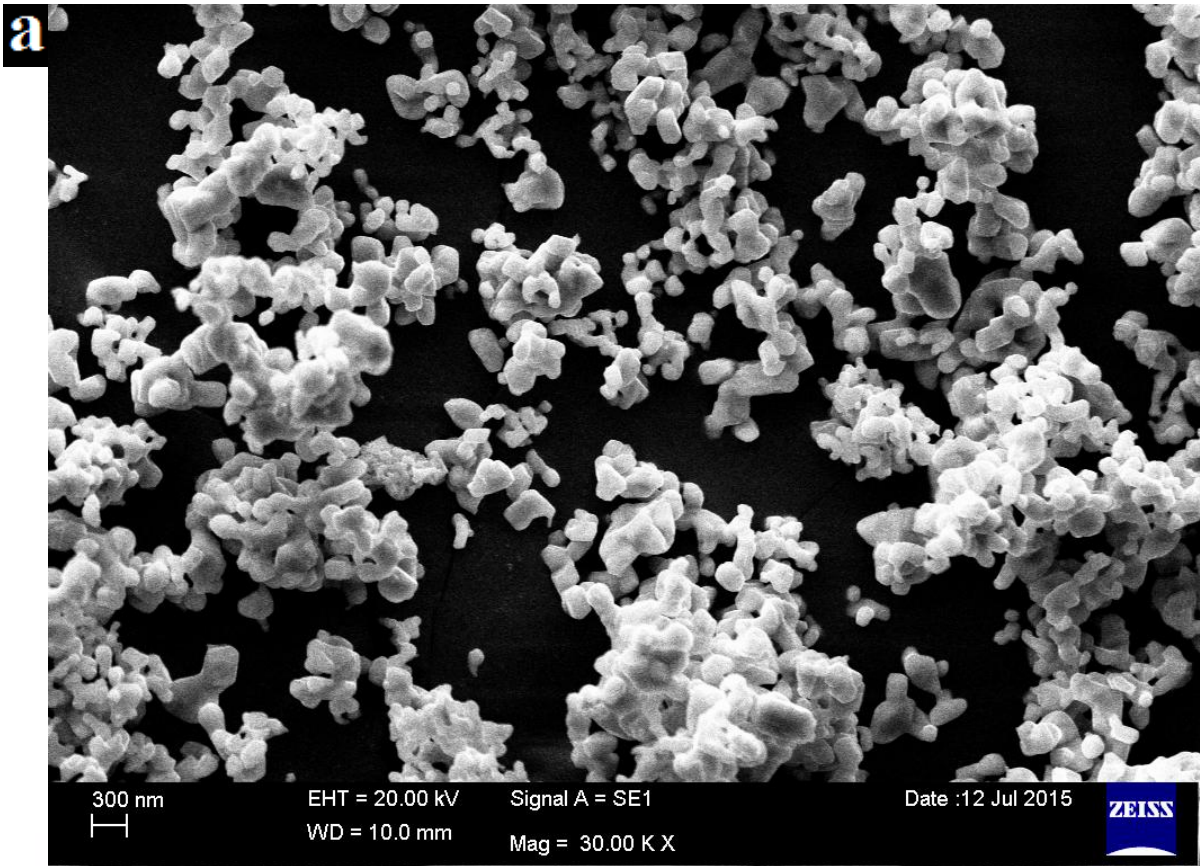






Fig.4 SEM images of  $Mn_3O_4$  nanoparticles (a) 1h (b&c) 12h (d) 24h

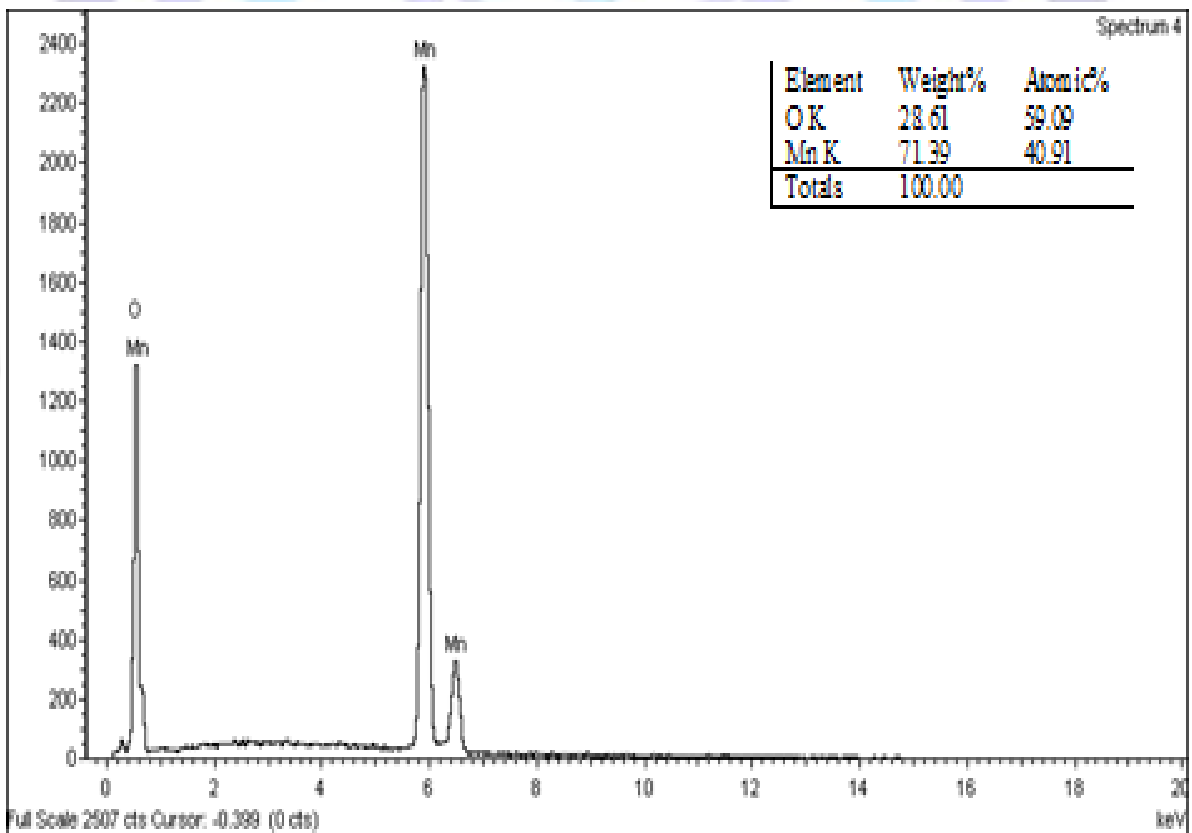


Fig.5 EDAX spectrum of  $Mn_3O_4$  nanoparticles

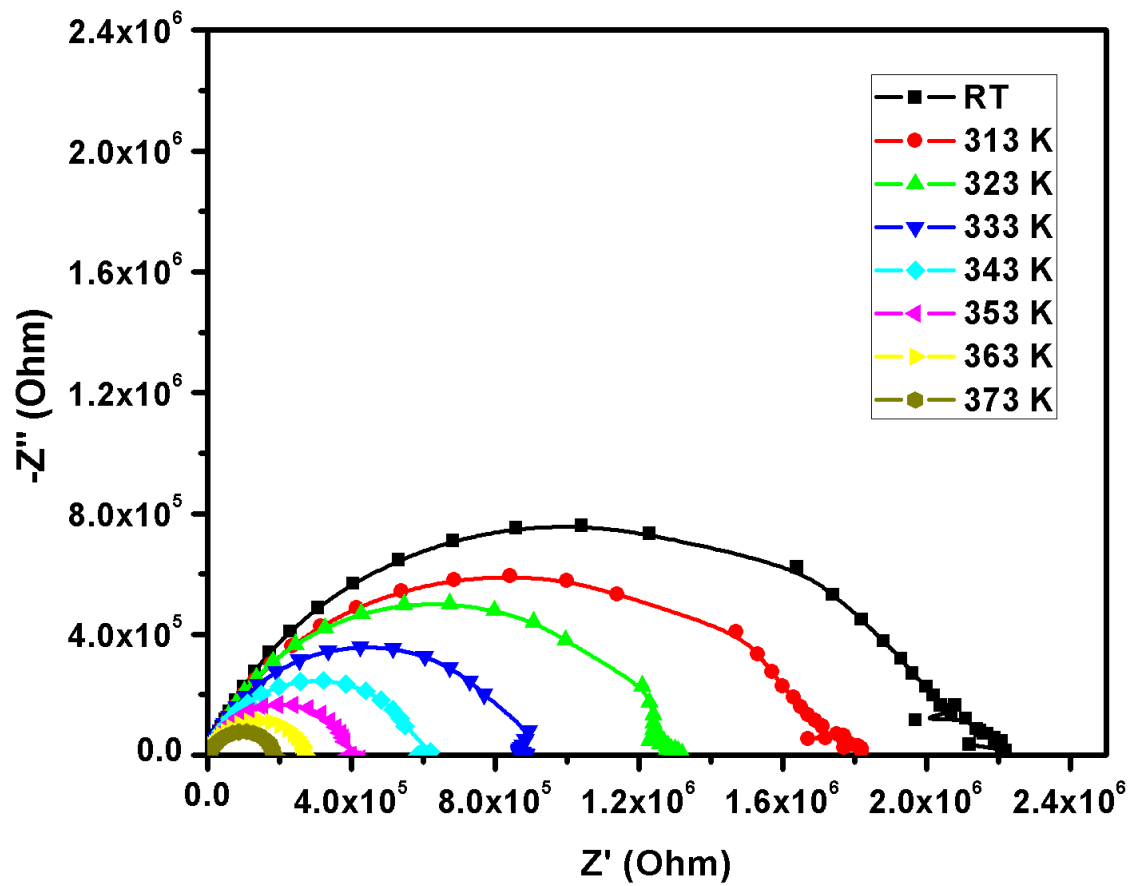


Fig. 6 Cole-Cole plots of Mn<sub>3</sub>O<sub>4</sub> nanoparticles

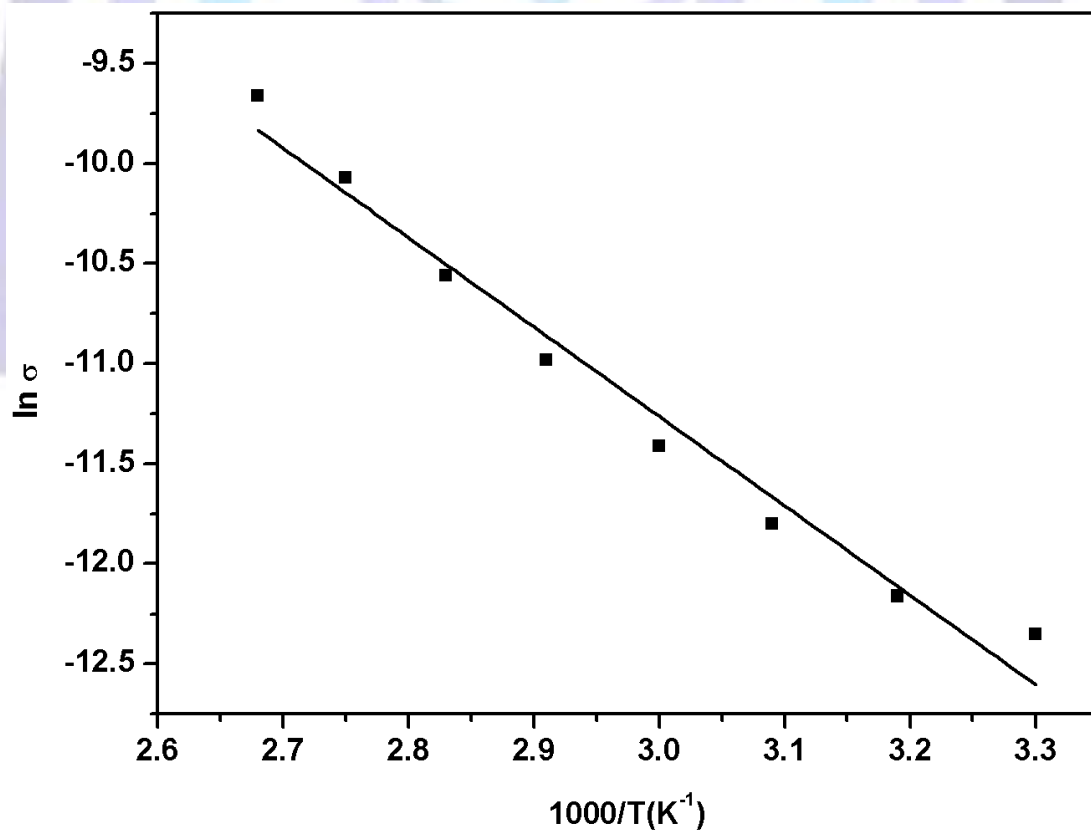


Fig. 7 Temperature dependence of conductivity

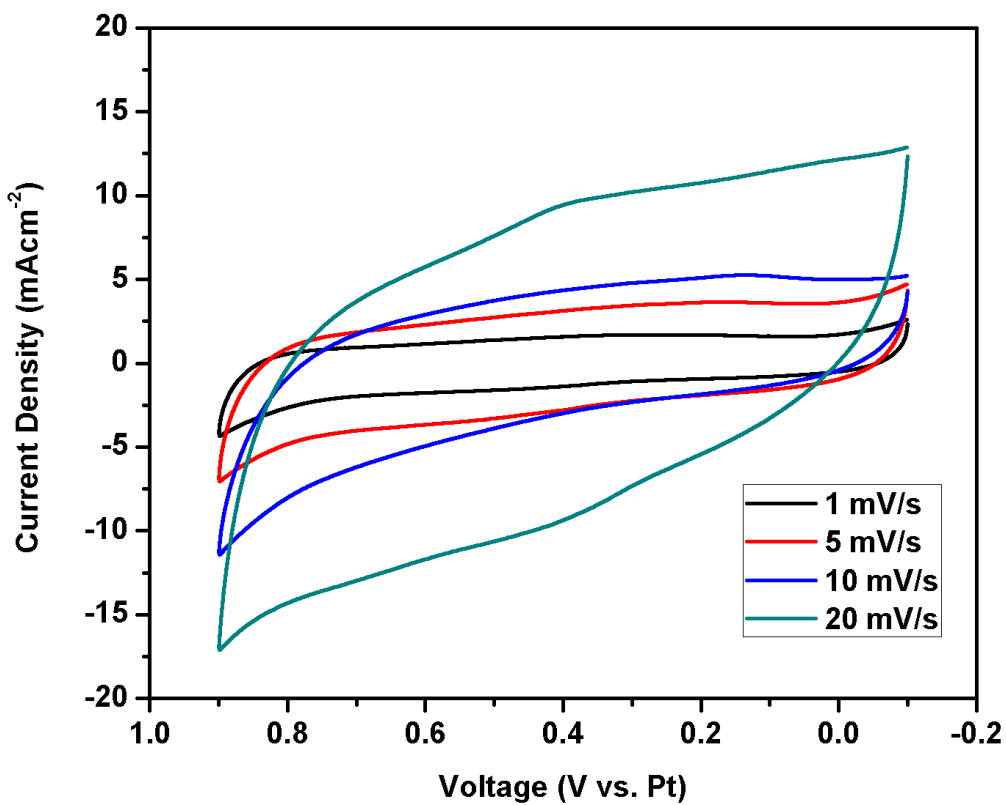


Fig. 8a The CV curves of  $Mn_3O_4$  electrode at different scan rates in the 1M  $Na_2SO_4$  electrolyte in the potential range -0.1V to +0.9 V

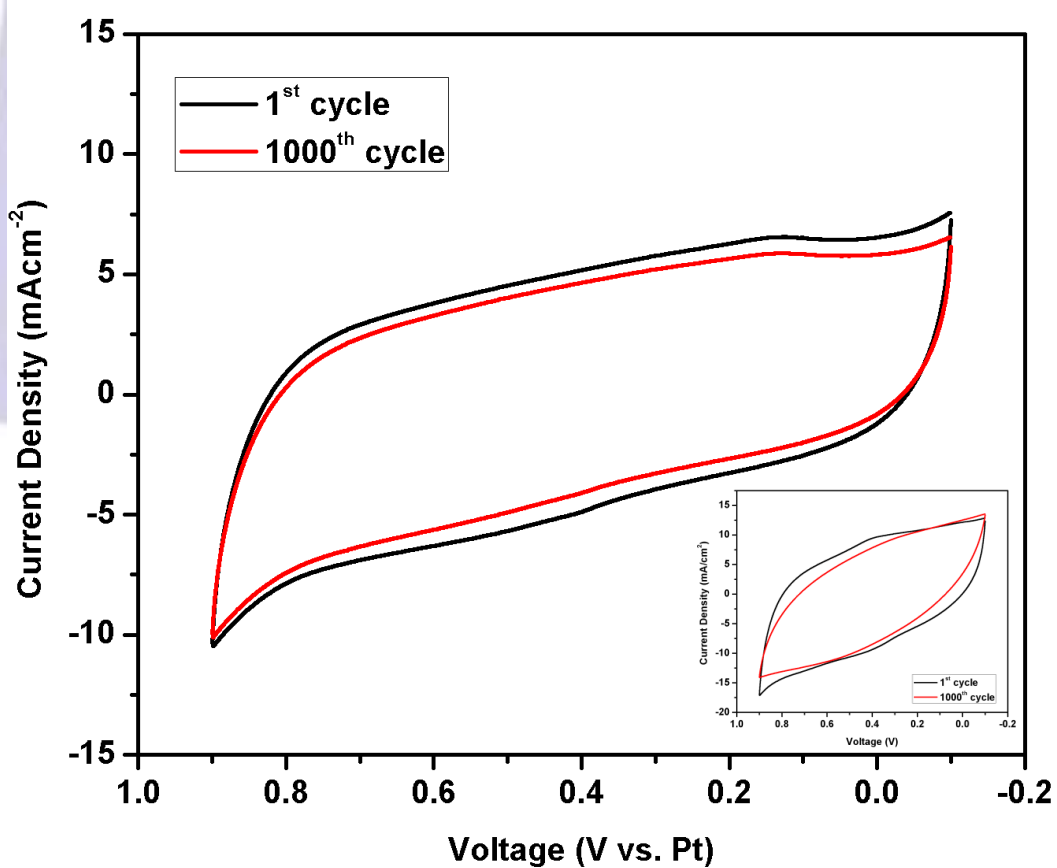


Fig. 8b The CV curves of  $Mn_3O_4$  for 1<sup>st</sup> and 1000<sup>th</sup> cycle at 10  $mVs^{-1}$  and 20  $mVs^{-1}$  (inset)

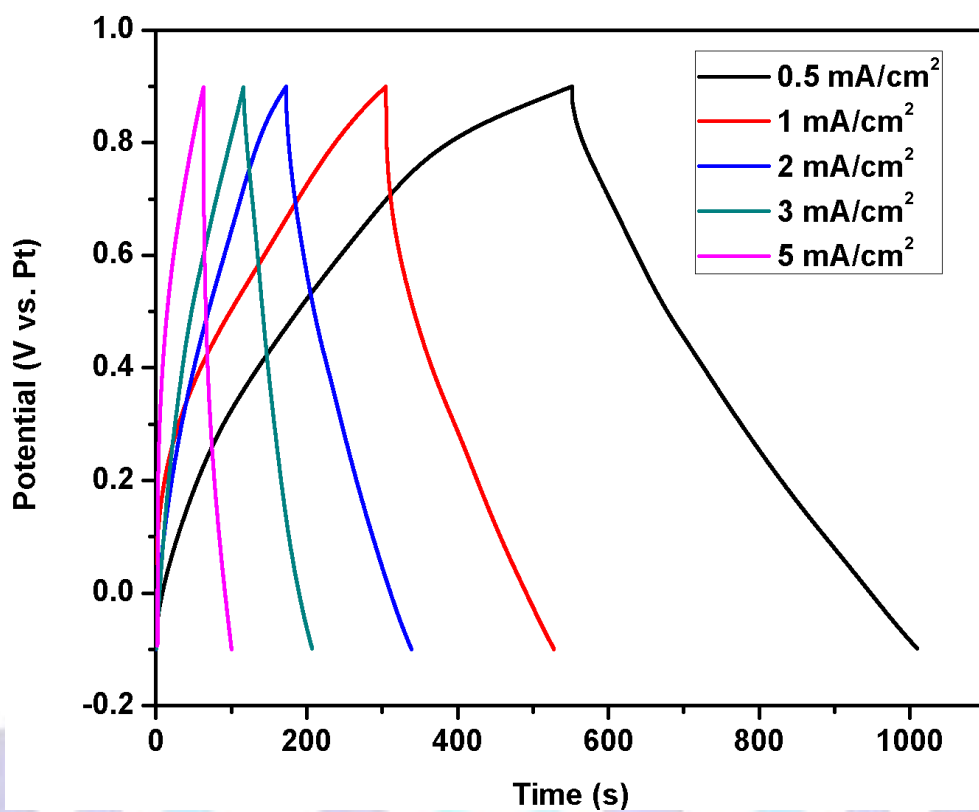


Fig. 9a Galvanostatic charge-discharge curves at different current densities 0.5 mAcm<sup>-2</sup>, mAcm<sup>-2</sup>, 2 mAcm<sup>-2</sup>, 3 mAcm<sup>-2</sup> and 5 mAcm<sup>-2</sup>

1

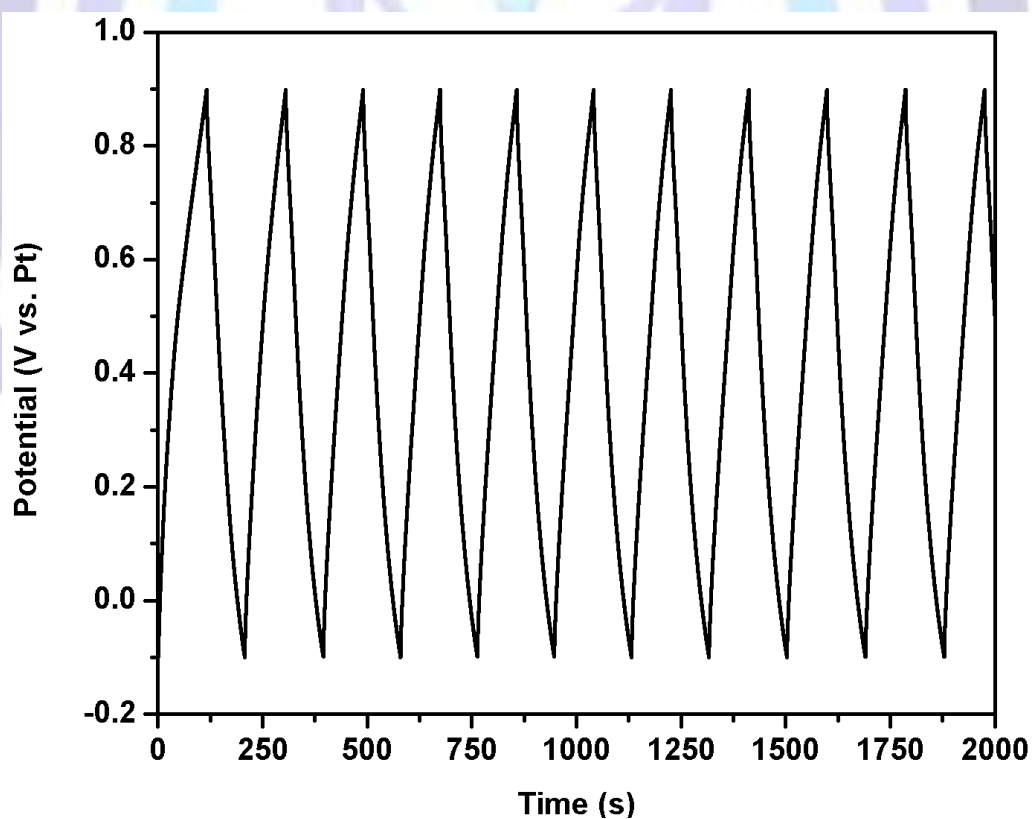


Fig. 9b First 10 charge-discharge cycles of Mn<sub>3</sub>O<sub>4</sub> nanoparticles in 1M Na<sub>2</sub>SO<sub>4</sub> electrolyte at a current density of 3 mAcm<sup>-2</sup>

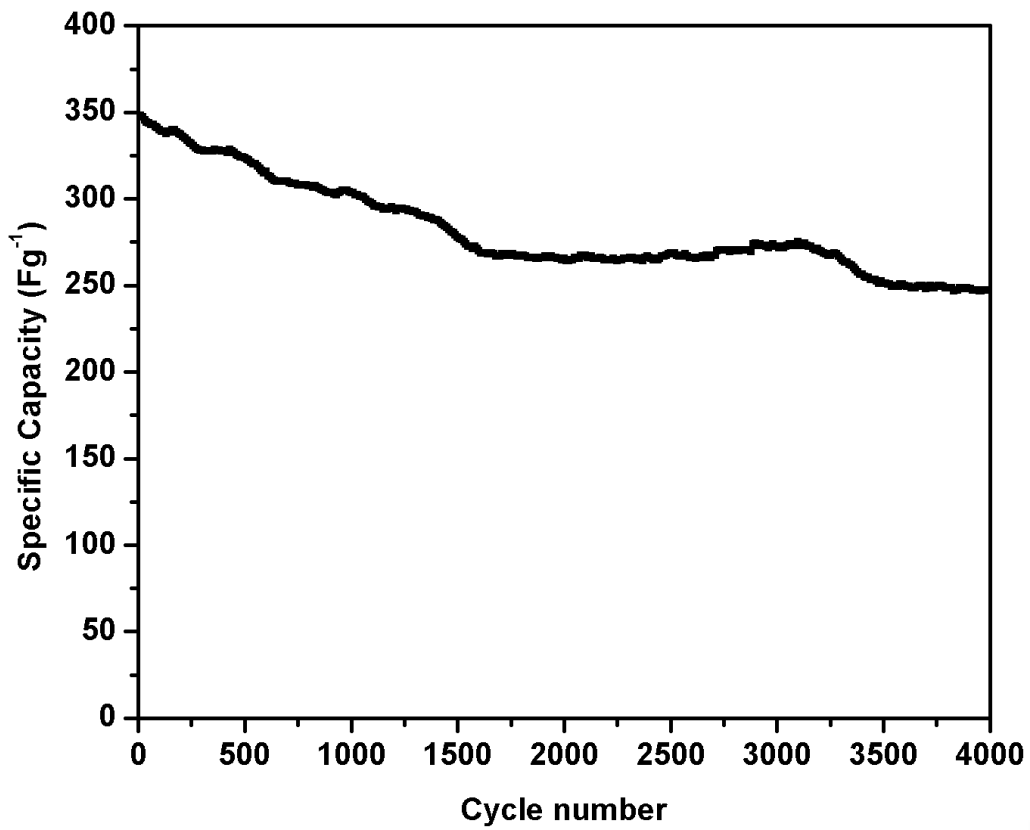


Fig. 9c Specific capacitance with cycle number

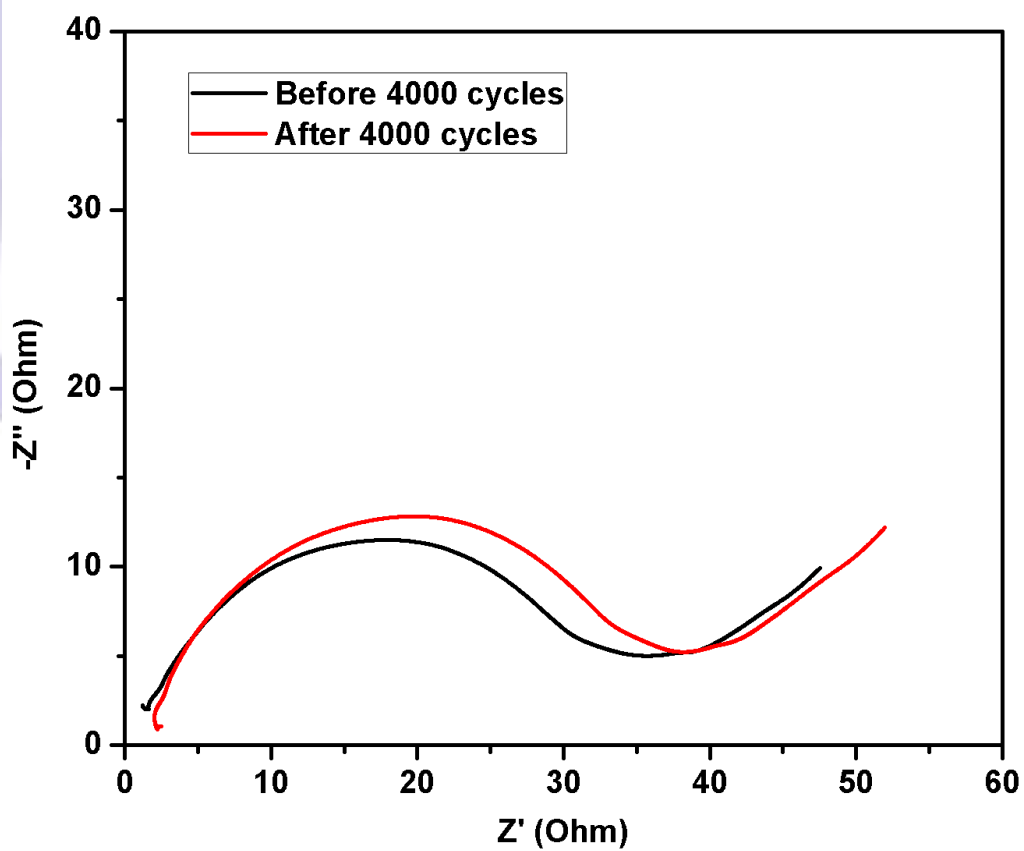


Fig. 10 Electrochemical Impedance Spectra of Mn<sub>3</sub>O<sub>4</sub> nanoparticles



## REFERENCES

- [1]. Kotz R, Carlen M. "Principles and applications of electrochemical capacitors" *Electrochim Acta* 45 (2000) 2483–2498.  
DOI: [10.1016/S0013-4686\(00\)00354-6](https://doi.org/10.1016/S0013-4686(00)00354-6).
- [2]. Hui Pan, Jianyi Li and YuanPing Feng "Carbon nanotubes for supercapacitor" *Nanoscale Research Letters* 5 (2010) 654-668.  
DOI: [10.1007/s11671-009-9508-2](https://doi.org/10.1007/s11671-009-9508-2)
- [3]. Chuang Peng, Shengwen Zhang, Daniel Jewell, George Z. Chen "Carbon nanotube and conducting polymer composites for supercapacitors" *Progress in Natural Science* 18 (2008) 777–788.  
DOI: [10.1016/j.pnsc.2008.03.002](https://doi.org/10.1016/j.pnsc.2008.03.002)
- [4]. Khomenk.Frackowiak Barsukov Béguin "Development of supercapacitors based on conducting polymers" *Springer* 229 (2006) 41-50  
DOI: [10.1007/1-4020-4812-2-4](https://doi.org/10.1007/1-4020-4812-2-4)
- [5]. Lokhande C.D, Dubal D.P Dubal, O.S. Joo "Metal oxide thin film based supercapacitors" *Current Applied Physics* 11 (2011) 255-270  
DOI: [10.1016/j.cap.2010.12.001](https://doi.org/10.1016/j.cap.2010.12.001)
- [6]. Devadas A, Baranton S, Napporn T.W, Coutanceau C "Tailoring of RuO<sub>2</sub> nanoparticles by microwave assisted Instant method for energy storage applications" *Journal of Power Sources* 196 (2011) 4044-4053.  
DOI [10.1016/j.jpowsour.2010.11.149](https://doi.org/10.1016/j.jpowsour.2010.11.149)
- [7]. Linrui Hou, Changzhou Yuan, Long Yang, Laifa Shen, Fang Zhang and Xiaogang Zhang "Urchin like Co<sub>3</sub>O<sub>4</sub> microspherical hierarchical superstructures constructed by one dimension nanowires towards electrochemical capacitors" *ACS Advances* 1 (2011) 1521-1526.  
DOI [10.1039/C1RA00312G](https://doi.org/10.1039/C1RA00312G)
- [8]. Han D, Xu P, Jing X, Wang J, Yang P, Shen Q, Liu J, Song D, Gao Z, Zhang M "Trisodium citrate assisted synthesis of hierarchical NiO nanospheres with improved supercapacitors performance" *Journal of Power Sources* 235 (2013) 45-53.  
DOI [10.1016/j.jpowsour.2013.01.180](https://doi.org/10.1016/j.jpowsour.2013.01.180)
- [9]. Wang B, Guan D, Gao Z, Wang J, Li Z, Yang W, Liu L "Preparation of grapheme nanosheets/SnO<sub>2</sub> composites by pre reduction followed by in situ reduction and their electrochemical performance" *Materials chemistry and physics* 141(1) (2013) 1-8.  
DOI [10.1016/j.matchemphys.2013.02.052](https://doi.org/10.1016/j.matchemphys.2013.02.052)
- [10]. Purushothan Reddy B, Sivajee Ganesh K, Jayanth Babu K, Hussain O.M, Julien. C M "Microstructure and supercapacitive properties of RF sputtered copper oxide thin films: Influence of O<sub>2</sub>:Ar ratio" *Ionics* (2015)  
DOI [10.1007/s11581-015-1403-5](https://doi.org/10.1007/s11581-015-1403-5)
- [11]. Zhang X, Yu P, Zhang D, Zhang H, Sun X, Ma Y "Room temperature synthesis of Mn<sub>3</sub>O<sub>4</sub> nanoparticles: characterization, electrochemical properties and hydrothermal transformation to γ-MnO<sub>2</sub> nanorods" *Materials Letters* 92 (2013) 401-404.  
DOI: [10.1016/j.matlet.2012.11.022](https://doi.org/10.1016/j.matlet.2012.11.022)
- [12]. Dubal DP, Dhawale DS, Salunkhe RR, Lokhande CD "A novel chemical synthesis of Mn<sub>3</sub>O<sub>4</sub> thin film and its stepwise conversion into birnessite MnO<sub>2</sub> during super capacitive studies" *Journal of Electroanalytical Chemistry* 647 (2010) 60-65.  
DOI: [10.1016/j.jelechem.2010.05.010](https://doi.org/10.1016/j.jelechem.2010.05.010)
- [13]. Nagamuthu S, Vijayakumar S, Muralidharan G "Synthesis of Mn<sub>3</sub>O<sub>4</sub>/Amorphous carbon nanoparticles as electrode material for high performance supercapacitor applications" *Energy and Fuels* 27 (2013) 3508-3515.  
DOI: [10.1021/ef400212b](https://doi.org/10.1021/ef400212b)energyfuels2013,27 3508-3515
- [14]. Xia H, Xiao W, Lai MO, Lu L "Facile synthesis of novel nanostructure MnO<sub>2</sub> thin film and their applications in supercapacitors" *Nanoscale Res letters* 4 (2009) 1035-1040.  
DOI [10.1007/s11671-009-9352-4](https://doi.org/10.1007/s11671-009-9352-4)
- [15]. Lin He, Geng Zhang, Yuanzhu Dong, Zhenwei Zhang, Shihan Xue, Xingmao Jiang "Polyetheramide Templated Synthesis of Monodisperse Mn<sub>3</sub>O<sub>4</sub> Nanoparticles with controlled size and study of the electrochemical properties" *Nano Micro Letters* 6(1) (2014), 38-45.  
DOI [10.5101/nml.v6i1.p38-45](https://doi.org/10.5101/nml.v6i1.p38-45)
- [16]. Fatemeh Davar, Masoud Salavati-Niasari, Noshin Mir, Kamal Saberyan, Majid Monemzadeh, Eshagh Ahmadi "Thermal decomposition route for synthesis of Mn<sub>3</sub>O<sub>4</sub> nanoparticles in presence of a novel precursor" *Polyhedron* 29(2010) 1747-1753  
DOI: [10.1016/j.poly.2010.02.026](https://doi.org/10.1016/j.poly.2010.02.026)
- [17]. Jiazheng Wang, Ning Du, Hao Wu, Hui Zhang, Jingxue Yu, Deren Yang "Order-aligned Mn<sub>3</sub>O<sub>4</sub> nanostructures as super high-rate electrodes for rechargeable lithium-ion batteries" *Journal of Power Sources* 222 (2013) 32-37.  
DOI [10.1016/j.jpowsour.2012.01.094](https://doi.org/10.1016/j.jpowsour.2012.01.094)
- [18]. Taher Yousefi, Ahmad Nozad Golikand, Mohammad Hossein Mashhadizadeh, Mustafa Aghazadeh "High temperature and low current density synthesis of Mn<sub>3</sub>O<sub>4</sub> porous nano spheres: characterization and electrochemical properties" *Current Applied Physics* 12(2012) 544-549.



DOI: 10.1016/j.cap.2011.08.018

[19]. Vijaya Sankar K, Kalpana D, Kalai Selvan R “ Electrochemical Properties of microwave-assisted reflux-synthesized  $Mn_3O_4$  nanoparticles in different electrolytes for supercapacitor applications” Journal of Applied Electrochemistry 42 (2012) 463-470.

DOI: 10.1007/s10800-012-0424-2

[20] Lu-Feng Y, Chuang G, Ming-Tao Z, Chao-Fan H, Jiang-Hu C, Ying-Liang L “Synthesis and Electrochemical properties of  $Mn_3O_4$  polyhedral nanocrystals” Chinese Journal of Inorganic Chemistry 29(2013) 381-388.

DOI: 10.3969/j.issn.1001-4861.2013.00.026

[21]. H. Jiang, T. Zhao, C.Y. Yan, J. Ma, C. Z. Li “ Hydrothermal synthesis of novel  $Mn_3O_4$  nano-octahedrons with enhanced supercapacitors performances” Nanoscale 2 (2010) 2195-2198

DOI: 10.1039/c0nr00257g

[22]. Gnana Sundara Raj B, Abdullah M. Asiri, Jerry, Wu J., Sambandam Anandan “ Synthesis of  $Mn_3O_4$  nanoparticles via chemical precipitation approach for supercapacitor application” Journal of Alloys and Compounds 636(2015) 234-240.

DOI 10.1016/j.jallcom.2015.02.164

[23]. H Jiang, T Zhao, C Yan, J Ma and C Li “Hydrothermal synthesis of novel  $Mn_3O_4$  nano-octahedrons with enhanced supercapacitors performances” Nanoscale 2 (2010) 2195-2198

10.1039/conr00257g

[24]. CM Julien, M. Massot, C. Poinson, Spectrochimica Acta A 60(2004) 689-700

[25]. Regmi R, Tackett R, Lawes G. “Suppression of low-temperature magnetic states in  $Mn_3O_4$  nanoparticles” Journal of Magnetism and Magnetic Materials 321 (2009) 2296-2299.

DOI: 10.1016/j.jmmm.2009.01.041

[26]. J. Zhao, C. Xu, Y Liu, and Y Qian “ crystallite size effects on the raman spectra of  $Mn_3O_4$ ” Nanostructured materials 10 (1998) 1331-1335

[27]. Shuang-Yu Liu, Jian Xie, Yun-Xiao Zheng, Gao-Shao Cao, Tie-Jun Zhu, Xin-Bing Zhao “Nanocrystal manganese oxide ( $Mn_3O_4$ , MnO) anchored on graphite nanosheet with improved electrochemical Li-storage properties” Electrochimica Acta 66 (2012) 271-278.

DOI 10.1016/j.electacta.2012.01.094

[28]. Ghodbane O, Pascal J L, Fraisse B, Favier F. “Structural in situ study of the Thermal behavior of Manganese dioxide material:Toward selected electrode materials for supercapacitors” ACS applied materials and Interfaces 2 (2010) 3493-3505

10.1021/am100669k

[29]. Dubal DP, Dhawale DS, Salunkhe RR, Fulari VJ, Lokhande CD “ chemical synthesis and characterization of  $Mn_3O_4$  thin films for supercapacitor application” Journal of Alloyed Compounds 497 (2010) 166-170

10.1016/j.jallcom.2010.02.182

[30]. H. Dhaouadi, O Ghodbane, F Hosni and F Touati (2012) ISRN spectroscopy 2012

DOI: 10.5402/2012/706398

[31]. Deepak P. Dubal and Rudoff Holze “A successive ionic layer adsorption and reaction(SILAR) method to induce  $Mn_3O_4$  nanospots on CNTs for supercapacitors” New Journal of Chemistry 37 (2013) 403-408.

10.1039/c2nj40862g